Journal of Materials Chemistry B

PAPER

View Article Online
View Journal | View Issue

Cite this: J. Mater. Chem. B, 2017, 5, 5176

Poly(L-lactide) melt spun fiber-aligned scaffolds coated with collagen or chitosan for guiding the directional migration of osteoblasts *in vitro*

Jianyong Feng,[ab] Deteng Zhang,[a] Meifang Zhu*[c] and Changyou Gao *[a]

Received 4th March 2017,
Accepted 26th May 2017

DOI: 10.1039/c7tb00601b

rsc.li/materials-b

Aligned fiber scaffolds can mimic the parallel aligned fibrils in the extracellular matrix (ECM) of bones, and thus regulate many cellular behaviors. The aligned scaffolds are usually prepared by a microplate micropatterned method, freeze casting, evaporation, slip casting, ice-templating, plain weaving, and fiber forming techniques. In this study, the melt spinning technology, which has the advantages of a higher spinning speed, solvent-free processing and readily scalable production, was used to prepare poly(L-lactide) (PLLA) melt spun fibers with an average diameter of 70.3 ± 11.4 μm. The fibers were further bonded by 5% PLLA tetrahydrofuran solution to prepare PLLA spun fiber-aligned scaffolds. Collagen and chitosan molecules were coated onto the fibers/into the scaffolds to obtain multiple biochemical and surface aligned topography cues, respectively. The collagen or chitosan-coated PLLA aligned scaffolds could effectively improve the viability, adhesion, length and migration behaviors of osteoblasts *in vitro*. In particular, the collagen coated aligned scaffold had the largest cell length and the fastest migration rate, with a preferential direction along the fibers. This type of scaffold provides a versatile substrate to control cell behaviors, having great potential for bone regeneration.

1. Introduction

The native extracellular matrix (ECM) is usually composed of fibrils ranging from tens of nanometers to micrometers in scale, and the organized structure of these matrix fibrils can guide tissue morphogenesis and remodeling.[1] Bone is a natural organic–inorganic composite consisting of collagen fibrils and embedded, well-arrayed, nanocrystalline, and rod-like inorganic materials.[2,3] Effective reconstruction of bone defects as a result of tumors, trauma, and periodontal disease is becoming a major challenge in tissue engineering,[4] in which the biomimetic structure of synthetic biomaterials plays a key role in guiding bone regeneration.[5] For the regeneration of highly organized structures, aligned scaffolds can provide biological cues which offer adequate topographic guidance to cells,[5] directing structural assembly of newly regenerated collagen fibers at the defect site for bone repair.[6] The highly parallel composite fibrous structure imitates collagen fibrils in natural bones,[7] and the ordered mineralization, oriented collagen type I fibrils and directed mineralization of bones are important prerequisites for mimicking *in vivo* bone formation.[8]

The aligned scaffolds can be prepared by a microplate micropatterned method,[9] freeze casting,[10] evaporation,[11] slip casting,[12] ice-templating,[13] plain weaving,[14] and fiber forming techniques.[15] The scaffolds of aligned fibers, which are usually produced by melt spinning,[16] dry spinning,[17] wet spinning,[18] dry–wet composite spinning[19,20] and electrospinning,[21] can mimic the morphology of collagen fibrils in the aligned structure of ECM.[2,3] Compared with other spinning methods, melt spinning has the advantages of higher spinning speed, solvent-free processes and potential of mass production.[16] Fibrous scaffolds with different topographical features can be easily obtained by regulating the fiber diameter, alignment, distribution and interfiber distance.[22] Surface topographic morphologies of fiber scaffolds, including fiber patterns, dimensions and mesh size, play an important role in regulating the cell behaviors.[22] The aligned fiber scaffold has a similar structure to the complicated chemical and physical crosslinking network of proteins and polysaccharides in ECM, guiding the cell growth direction and controlling cell behaviors with the well-known contact guidance effect.[23]

There are several methods to prepare the aligned fiber scaffolds, such as electrospinning,[24] centrifugal spinning,[25] melt-drawing,[26] unidirectional freeze-drying,[27] catalyst-free chemical vapor deposition,[28] 3-dimensional (3D) extrusion[29]

[a] MOE Key Laboratory of Macromolecular Synthesis and Functionalization, Department of Polymer Science and Engineering, Zhejiang University, Hangzhou 310027, China. E-mail: cygao@mail.hz.zj.cn
[b] College of Materials and Textiles, Zhejiang Sci-Tech University, Hangzhou, Zhejiang 310018, China
[c] College of Materials Science and Engineering, Donghua University, Shanghai 201620, China. E-mail: zmf@dhu.edu.cn

and bidirectional freezing techniques.[30] Deepthi *et al.*[24] prepared layered chitosan–collagen hydrogel/aligned poly(L-lactide) (PLLA) nanofibers for flexor tendon regeneration by the electrospinning method. Wang *et al.*[25] manufactured aligned poly(vinyl pyrrolidone) (PVP) fiber scaffolds as matrix type antibiotic drug delivery systems by the centrifugal spinning technique. Tan *et al.*[26] used the melt-drawing method to prepare aligned poly(L-lactide-*co*-ε-caprolactone) (PLCL) fibrous and tubular scaffolds. Fereshteh *et al.*[27] prepared aligned porous poly(ε-caprolactone) (PCL)/zein scaffolds as drug delivery systems *via* the improved unidirectional freeze-drying method. Kazantseva *et al.*[28] produced graphene-augmented nanofiber aligned scaffolds to study the behaviors of human mesenchymal stem cells. Moon *et al.*[29] prepared 3D alumina/camphene aligned porous scaffolds with a biomimetic macro/microporous structure. Bai *et al.*[30] prepared a scaffold by bidirectional freezing, which was used as a promising new bone substitute material.

The aligned fiber scaffolds produced by electrospinning have been applied in bone regeneration. For example, Stachewicz *et al.*[31] prepared poly(D,L-lactide-*co*-glycolide) (PLGA) nanofiber aligned scaffolds to study the interaction between osteoblast spreading, filopodia, gene expression, proliferation and nanofiber surfaces. Moon *et al.*[29] produced 3D ceramic/camphene-based extrusion of alumina bone scaffolds with an aligned porous structure to evaluate the biocompatibility of MC3T3-E1 cells, such as attachment and cell viability. Perikamana *et al.*[6] fabricated PLLA electrospun nanofibers with an aligned morphology to investigate cell adhesion, *in vitro* osteogenic differentiation, histological and immunohistochemistry for bone regeneration, and found that the aligned fibers can be used for engineering bone tissues with structurally assembled collagen fibers and a defined direction. Samavedi *et al.*[32] demonstrated that the difference in the alignment of PCL fibers affects the morphology and orientation of cells in bone regeneration. The aligned scaffolds cause significant changes in osteoblast growth behaviors and gene expression, demonstrating that the osteoblast phenotype is maintained, and the aligned fibers provide rapid osteoblast growth for more superficial repair.[31] The aligned scaffolds permit cell adhesion, and can function as substrates for the development of bone tissue engineering.[33] *In vivo* bone formation and histology in the aligned scaffolds show ordered, unidirectional alignment of collagen assembly that resembles the collagen assembly of a lamellar bone, which also results in anisotropic mechanical behavior of new bones.[6]

Special surface modification techniques for biomaterials such as vapor based polymer coating, plasma, plasma-induced micropatterning, plasma and photons, ion sputtering, and plasma-based ion-implantation, *etc.* have been used to improve the hydrophilicity and modulate cell behaviors.[34] There are several ways to obtain surface coatings such as thermal spraying, sputtering, pulsed laser deposition, dynamic hybrid coating, dip coating, sol–gel coating, electrophoretic deposition, hot isostatic pressing and solution deposition.[35,36] Among them, solvent coating, *i.e.* immersing scaffolds in a polymer solution for a sufficient time, has the merits of simplicity, versatility, and low cost.[37] Surface coating can enhance cell growth and differentiation *in vitro*,[38] attenuate the inflammatory process, and increase the osteointegration and osteoinduction properties *in vivo*.[39]

In this paper, PLLA melt spun fibers are produced, which are further manufactured into a fiber-aligned structure (Fig. 1). After physical bonding by PLLA tetrahydrofuran solution, the PLLA melt spun fiber-aligned scaffold is obtained. Then the aligned scaffold is further coated by collagen and chitosan, whose influences on the osteoblasts in terms of cytoviability, morphology and migration are investigated.

2. Experiments

2.1 Preparation of PLLA melt spun fibers by 24 orifices

PLLA polymer particles purchased from Jinan Daigang Biomaterial Co. Ltd (Jinan, China) were dried at 60 °C for 24 h using a vacuum drum dryer (JM-500 ZGX, Shanghai Daphne Rose Kingma Electro-optical Technology Research Institute, China) to remove moisture. The polymers were fed using a charging machine (JM-QZJ, Shanghai Daphne Rose Kingma Electro-optical Technology Research Institute, China) in a screw extruder. The polymers were melt-spun at 225, 233, 230 and 233 °C temperature zones for each part of the MFG NO. A-228 screw extruder (Tokyo, Japan), and then extruded by a 24 orifice which had 0.3 mm nozzle hole diameter (D) and a 3 : 1 length (L) to diameter ratio to produce the PLLA melt spun fibers. The fibers were winded at 70 m min^{-1} winding speed on the take-up roll (Fig. 1a).

2.2 Preparation of PLLA melt spun fiber-aligned scaffolds

A YG086 measuring reel purchased from Changzhou first textile equipment Co., Ltd (Changzhou, China) with 100 r min^{-1} rotating speed, 1000 mm reel circumference and 3.5 cm width was used to prepare parallel PLLA melt spun fibers. The aligned PLLA fibers were glued by PLLA solution. 1 g PLLA was dissolved in 20 mL tetrahydrofuran by stirring for a long time to prepare 5% (wt v^{-1}) PLLA tetrahydrofuran solution. A brush was fully immersed in this 5% PLLA tetrahydrofuran solution for 2 s, and then brushed lightly on the surface of parallel PLLA fibers. The wet aligned scaffolds were put in a fume cupboard for 24 h to fully evaporate tetrahydrofuran. The dry PLLA aligned scaffolds (Fig. 1b) were divided into three groups, and two of them were used for collagen and chitosan coatings, respectively.

2.3 Preparation of collagen and chitosan-coated aligned scaffolds

The concentrations of collagen and chitosan were chosen for the purpose of coating as much collagen and chitosan on the fiber surface as possible, while preserving the clear fiber structure. According to the molecular weight and viscosity of the collagen and chitosan solutions, herein 1% chitosan (less viscous) and 0.5% collagen (higher viscous) were used, respectively. At these concentrations, the fiber surface can be successfully covered, while the inner fiber structure can be preserved.

2 mL 99.5% acetic acid was mixed with 98 mL deionized water to prepare 2% (v/v) acetic acid solution, into which 0.5 g collagen, which was extracted from bovine tendon in our lab,[40]

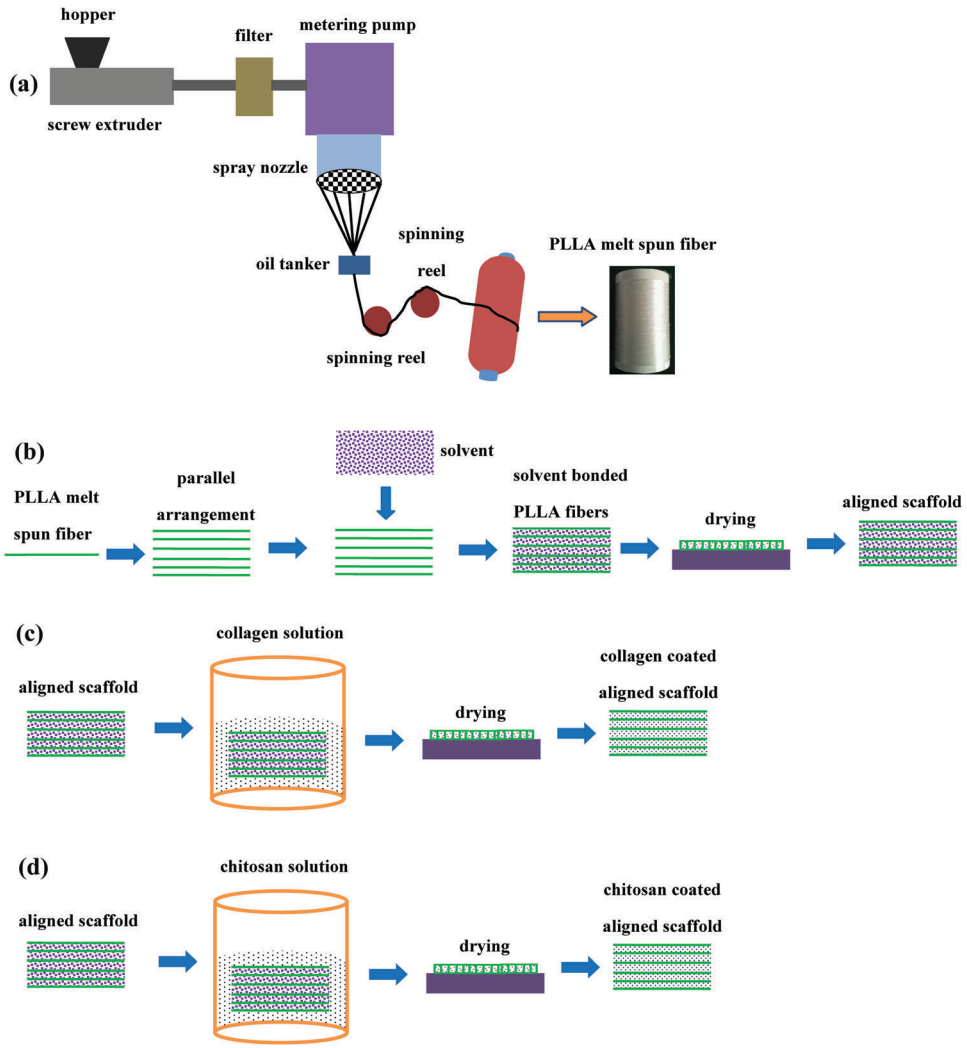

Fig. 1 Schematic of the processes used to prepare PLLA melt spun fibers (a) and solvent bonded PLLA melt spun fiber-aligned scaffold (b), collagen-coated PLLA melt spun fiber-aligned scaffold (c), and chitosan-coated PLLA melt spun fiber-aligned scaffold (d).

was dissolved to form a 0.5% (wt v^{-1}) collagen solution. The aligned scaffold was completely submerged in the 0.5% collagen solution for 3 h. The aligned scaffold was put in a fume cupboard for 24 h, and then dried at 37 °C in a drying oven for 3 h to obtain a completely dried collagen-coated aligned scaffold (PLLA–collagen, Fig. 1c).

Chitosan (DAC > 85%, Jinan Haidebei Marine Bioengineering Co. Ltd Shandong, China) was dissolved in 2% acetic acid solution to prepare 1% (wt v^{-1}) chitosan solution.[41] The aligned PLLA scaffold was similarly treated with the chitosan solution to obtain a chitosan-coated aligned scaffold (PLLA–chitosan, Fig. 1d).

2.4 Characterization of aligned scaffolds

In order to obtain a small sample, a 0.5 × 0.5 cm portion was cut from the whole scaffolds. The ETD-2000 sputtering apparatus was used for gold plating the small samples two times, each for 50 s. Then an S-4800 scanning electron microscope (SEM, Hitachi) was used to observe the surface morphology of the scaffolds. The cross-sectional morphology of the scaffolds was analyzed directly from the cross section. The samples were frozen in liquid nitrogen for about 3 min, and were cut by a blade perpendicular to the longitudinal direction. Image J software (National Institutes of Health, USA)[42] was applied to measure the distance between two adjacent fibers from the surface morphology of SEM, which could be considered as the pore diameter of the scaffolds.

According to Nisbet,[43] Guo,[44] Ayres[45] and Lee,[46] the value of the alignment degree could be measured using Image J software from SEM images. It was necessary to draw a straight line which was parallel to the *x*-axis along the horizontal direction of the scaffolds. Then the angle formed between the fiber orderly arrangement direction and the horizontal straight line direction was used to express the alignment degree of fibers.

The scaffold thickness was measured using a Vernier caliper at five different positions.

The process of the liquid displacement method for measuring the porosity has been stated in detail in Nazarov's research,[47] and ethanol was used as the displacement liquid to measure the porosity.

An Instron 5540A mechanical universal testing machine from American Instron company was used to measure the stress (σ, MPa) and strain (ε, %) of the scaffolds at 100 mm min^{-1} speed. The scaffolds were cut in a size of 6 cm^2 and the clamping length was 4 cm^2.

The static water contact angle of the samples was measured using a DSA100 contact angle measuring system (Krüss, Germany). The samples were cut into a size of 8 cm^2, and then placed on the surface of a glass slide by double-sided adhesive tape to ensure a flat surface. A 5 μL water droplet was placed onto the sample surface, and its image was captured and analyzed after about 15 s.

The contents of N, C and H elements of the samples were measured by elemental analysis (VarioMICRO equipment, Elementar Analysensysteme Gmbh, Germany) under conditions of 2 mg sample, 950 °C combustion tube temperature and 80 s oxygen filled time. To study the stability of collagen and chitosan coatings on the fiber surface, the samples were incubated in PBS at 37 °C for 1, 3 and 7 d, and then dried at 37 °C for 1 d in an oven before measurements.

2.5 Cell experiments

According to ref. 48 and 49, the cell culture medium consisted of 90% minimum essential medium alpha (MEMα, Gibco), 10% fetal bovine serum (FBS, purchased from American life technology company) and 100 U mL^{-1} penicillin and 100 μg mL^{-1} streptomycin with a pH value of 7.4. MC3T3-E1 osteoblasts purchased from the Cell Bank of Typical Culture Collection of the Chinese Academy of Sciences (Shanghai, China) were cultured in this medium at 37 °C in a 5% CO_2 humidified environment. The aligned scaffolds were firstly cut into small pieces evenly and placed in a well of a 24-well tissue culture plate, and were sterilized under ultraviolet radiation for 30 min before cell experiments.

2.6 Cell nucleus and actin fiber staining

The cells were seeded onto the scaffolds at 1×10^5 cells per mL density and incubated for 24 h in a well of a 24-well culture plate, and then were carefully washed with PBS 3 times and fixed with 4% paraformaldehyde at 37 °C for about 30 min, followed by 3 washes with PBS. The cells were further treated with 0.5% (v/v) Triton X-100/PBS at 4 °C for 10 min to permeabilize the cell membrane. After being rinsed with PBS, they were incubated in 1% bovine serum albumin (BSA)/PBS at 37 °C for 1 h to block the nonspecific interactions. Then the cells were incubated with a mouse monoclonal antibody against human 67LR (Abcam) for 1 h. After being washed with 1% BSA/PBS, they were further stained with FITC-labeled goat antimouse IgG (Beyotime, China) and 4′,6-diamidino-2-phenylindole (DAPI) (Sigma) at room temperature for 1 h, followed by 3 washes with PBS.[50] The cells were observed under a confocal laser scanning microscope (CLSM, LSM 510, Carl Zeiss).

2.7 Cell length and growth angle

Fluorescein diacetate (FDA) was purchased from Aldrich-Sigma (St. Louis, USA). 50 mg FDA was dissolved in 10 mL acetone to prepare a 5 mg mL^{-1} FDA solution. The cells were seeded at 5×10^4 cells per mL density and incubated for 24 h. Then a 20 μL 5 mg mL^{-1} FDA solution was injected into each well and incubated for 5 min, and then the cells were washed with PBS 3 times for fluorescence microscopy (FM) observation and measurement of the cell length and growth angle.

The cell length could be measured using Image J software from the FM images. The cell length defined as the straight line distance from one end to the other end of a cell. For the non-linear shape cell, the length was defined as the maximum linear distance between two ends of a cell.[51]

The angles of cell alignment to the x axis were analyzed by using Image J software.[52] The angles between the cell growth direction and the fiber parallel arrangement direction could then be obtained.

2.8 Cytoviability assay

Cell viability was determined by the 3-[4,5-dimehyl-2-thiazolyl]-2,5-diphenyl-2-*H*-tetrazolium bromide (MTT) assay[53] with a low density of 5×10^3 cells per mL after being incubated for 1 d and 7 d. After the cells were incubated with 1 mL MTT mixtures which had 800 μL cell culture medium and 200 μL MTT solution (5 mg mL^{-1}) for 3–4 h, the culture media were discarded, and each sample was incubated in 100 μL dimethyl sulfoxide (DMSO) for about 15 min. When the crystal was sufficiently dissolved, aliquots were pipetted into a 96-well plate to quantify the absorbance (optical density, OD) at 570 nm by a microplate reader (Tecan M200 PRO, Tecan company, Switzerland). The OD value was proportional to the cytoviability.[54]

2.9 Cell migration

The cells were seeded on the scaffolds at a density of 1×10^6 cells per mL. 12 h later the cell migration traces were recorded for 12 h under a time-lapse phase-contrast microscope (DMI6000B, Leica) equipped with an incubation chamber (95% air and 5% CO_2 at 37 °C). Image J software was employed to trace each individual cell *in situ*, and thus a variety of (x, y) position coordinates were exported over the observation time period with the manual tracking plugins.[52]

MC3T3-E1 osteoblast trajectories were reconstructed from the center positions of individual cells, and the initial position of each single cell was automatically defined as the original position (0, 0). The cell migration distance S was then calculated using a Chemotaxis Tool (Ibids, Germany) with a 15 min time interval according to the following equations. All mitotic and spherical dead cells were excluded from the analyses. At least 50 cells were chosen randomly from each sample for analysis.[52,55]

$$S = \sum_{i=1}^{t=12} \sqrt{(x_i - x_{i-1})^2 + (y_i - y_{i-1})^2}$$

The cell migration rate was obtained from $v = S/t$.[52]

2.10 Statistical analysis

The experimental data were expressed as mean ± standard deviation, and the significant difference between groups was analyzed by using one-way analysis of variance (ANOVA)

(for two groups) and two-way ANOVA (for more than two groups) in the Origin 8.0 software. The statistical significance was set as $p < 0.05$ and $p < 0.01$, respectively.[56]

3. Results

3.1 Structure and properties of PLLA melt spun fibers

The diameter of PLLA melt spun fibers prepared by 24 orifices was 70.3 ± 11.4 μm. It could be found that these fibers had a smooth surface and a circular cross section (Fig. 2). The surface and cross-sectional morphology of PLLA melt spun fibers in our research was consistent with those reported previously.[57,58]

3.2 Surface and cross-sectional morphology of aligned scaffolds

After solvent bonding with the PLLA solution, the aligned PLLA fibers were bonded together to form integrate scaffolds (Fig. 3a–c), and the adhesive PLLA molecules on the fiber surface are noticeable (Fig. 3b). The robust bonding enabled the further surface coating of the fibers in the scaffolds by collagen solution and chitosan solution without destroying the intact structure of the scaffolds, respectively. The fibers in all the PLLA–collagen and PLLA–chitosan aligned scaffolds remained in an aligned direction without significant change (Fig. 3d–i). Compared with the PLLA aligned scaffold, the PLLA–collagen aligned scaffold had a more smooth fiber surface (Fig. 3e), while the PLLA–chitosan aligned scaffold retained a rougher fiber surface (Fig. 3h). The cross-sectional morphologies of the aligned scaffolds had no significant difference, and all of them showed obvious vacancies throughout the scaffolds, suggesting good pore interconnectivity. The porous structure could improve cell in-growth, facilitate neovascularization from the surrounding tissues, increase the diffusion effect of nutrients and gases, and remove metabolic wastes more easily.[59]

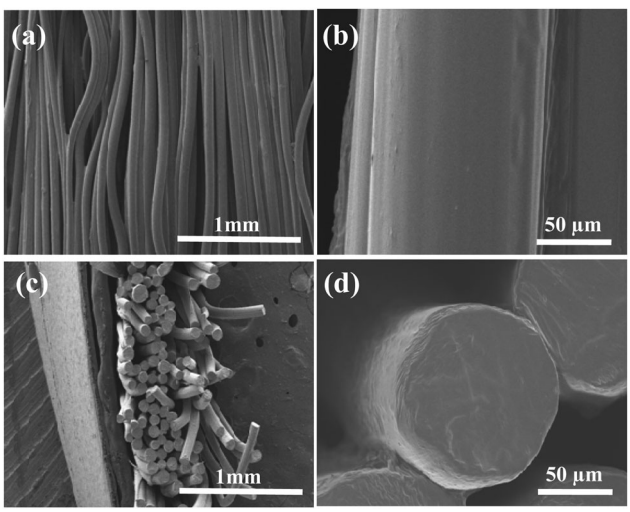

Fig. 2 SEM images showing (a) and (b) surface morphology, and (c) and (d) cross-sectional morphology of PLLA melt spun fibers.

3.3 Physical and surface chemical properties of aligned scaffolds

The fibers in all the three aligned scaffolds had a good orderly arrangement (Fig. 4a), and most of the fibers exhibited parallel alignment angles lying between 85° and 90° (the highest alignment degree is 90°, *i.e.* perpendicular to the *x*-axis[4]). Comparatively, the alignment degree of PLLA–collagen scaffolds was significantly better than that of PLLA scaffolds ($p < 0.01$) and PLLA–chitosan scaffolds ($p < 0.01$), whereas the alignment degree between PLLA–chitosan scaffolds and PLLA scaffolds did not show significant difference ($p > 0.05$). The wetting of the fibers and coating of macromolecules may change the curvature and thereby the orientation of the fibers, leading to a slight change in the alignment degree. We consider this to be basically engineering process-driven, and hence may rather be stochastic.

After collagen and chitosan coating, the aligned scaffolds had a smaller pore diameter ($p < 0.05$) and porosity, which were the smallest for the PLLA–collagen scaffold (Fig. 4b and c). It is known that the collagen and chitosan molecules could retain on the surface of the PLLA melt spun fibers and in the pores of the scaffolds, leading to a decrease in the pore diameter and porosity. This is the usual case for other types of fibers coated with collagen[60] or chitosan.[61] Analysis in conjunction with the surface and cross-sectional morphology of the aligned scaffolds shows that the collagen molecules could more easily adhere onto the PLLA fibers and retained into the PLLA melt spun scaffolds.

The thickness of the aligned scaffolds cultured under 37 °C and 5% CO_2 conditions after 1, 3, 5, and 7 d showed no apparent change (Fig. 4d), implying that these three aligned scaffolds had robust stability and a favorable bonding effect among fibers. Therefore, the robust structure of the aligned scaffolds could guarantee the accuracy of cell experiments.

After collagen and chitosan coating, the stress of the aligned scaffolds had different degrees of improvement ($p < 0.01$) (Fig. 5a) due to the binding effect of the coated molecules between the fibers, which is more prominent for the collagen coating and hence a larger improvement of stress. The coating of biomacromolecules enabled better surface wettability, as demonstrated by the smaller water contact angles, especially on the PLLA–collagen scaffolds compared to that on the PLLA aligned scaffolds (Fig. 5b). The better hydrophilicity can only be attributed to the coated collagen or chitosan, which is consistent with the observation of Douglas *et al.*[62]

To study the stability of the coated collagen or chitosan after incubation in medium, the contents of N, C and H elements of the scaffolds were measured by elemental analysis (Table 1).[63,64] The N element can only be contributed by collagen or chitosan, and hence is proportional to the content of collagen or chitosan. After 1 d incubation, the biomacromolecules were released sharply, and then remained unchanged up to 7 d (Table 1). These results suggest that some of the collagen or chitosan molecules can stably adhere onto the PLLA fibers, enabling the relatively long term maintenance of the surface modification for cell culture, although pretty many loosely attached ones are quickly rinsed at the very initial stage.

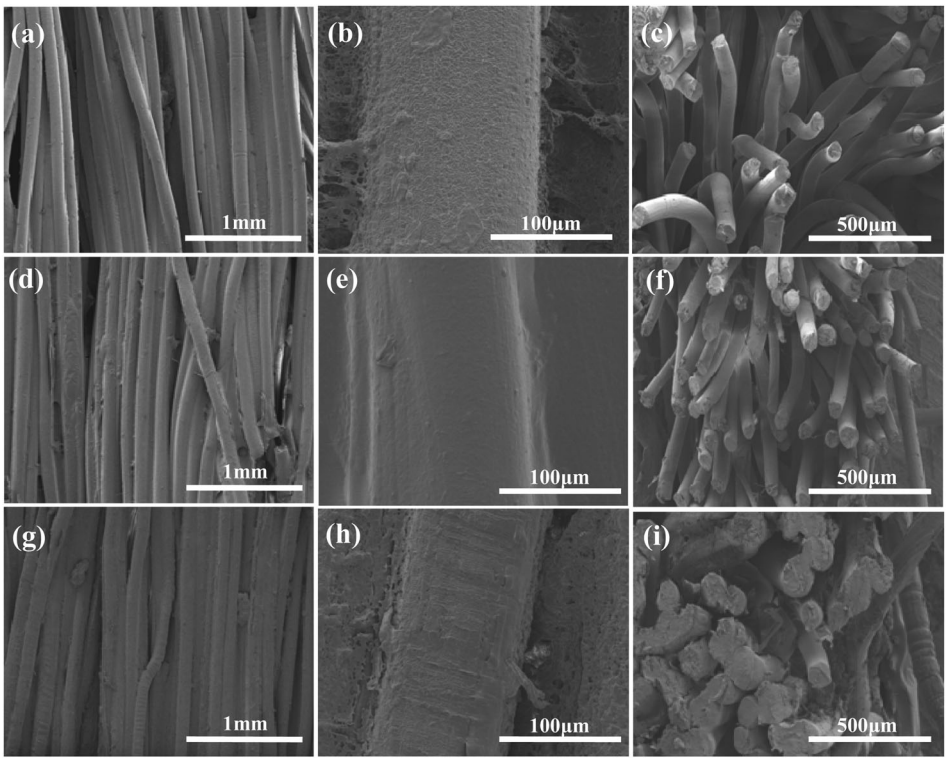

Fig. 3 SEM images of (a)–(c) solvent-bonded PLLA aligned scaffold, (d)–(f) PLLA–collagen aligned scaffold, and (g)–(i) PLLA–chitosan aligned scaffold. (b), (e), and (h) single PLLA fiber in different scaffolds. (c), (f), and (i) cross-sectional morphology of different scaffolds.

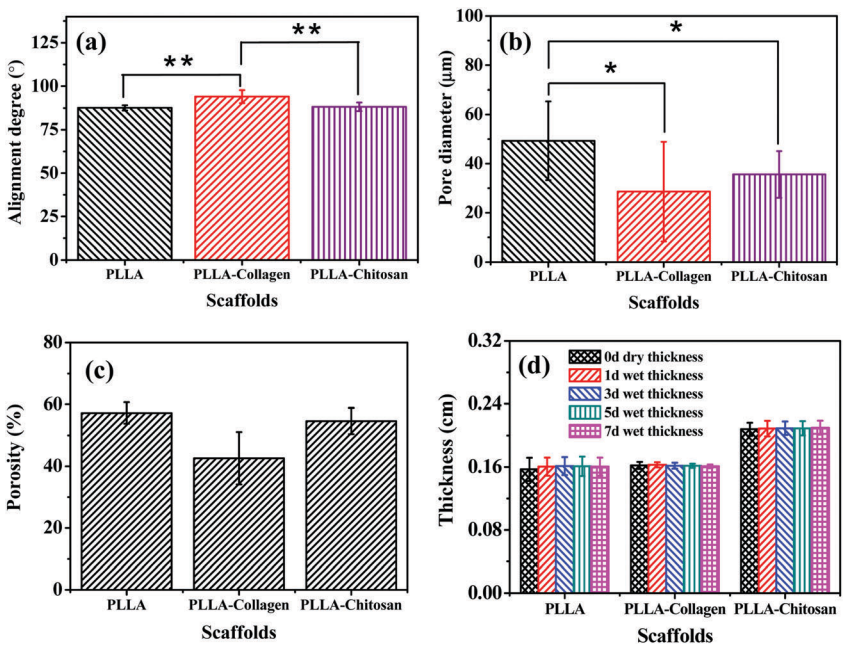

Fig. 4 (a) Alignment degree (N = 10), (b) pore diameter (N = 10), and (c) porosity (N = 3). (d) Thickness of aligned scaffolds after being incubated for 1, 3, 5 and 7 d (N = 5). * and ** indicate significant difference at $p < 0.05$ and $p < 0.01$, respectively.

It is known that collagen contains different types of cell-binding domains such as RGD peptides,[65] while both collagen and chitosan are positively charged, which can enhance the interactions between cells and substrates. By contrast, due to the rather hydrophobic surface of the PLLA substrate, and the lack of motifs for cell binding, the PLLA fibers alone are not able to form active interactions with cells. The combination of collagen or chitosan with the PLLA-aligned scaffolds hence

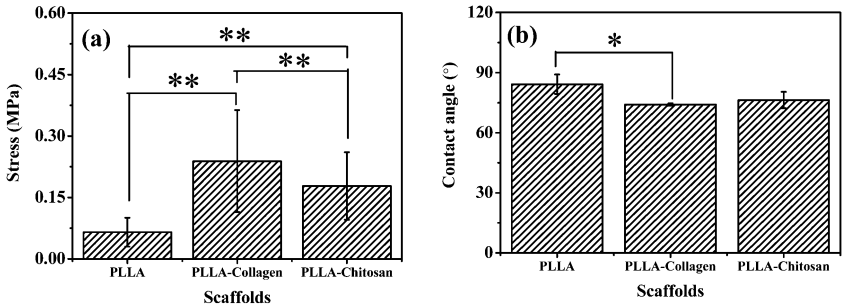

Fig. 5 (a) Stress and (b) water contact angle (N = 3) of the aligned scaffolds. * and ** indicate significant difference at $p < 0.05$ and $p < 0.01$, respectively.

Table 1 N, C and H elements of different scaffolds after incubation for different period of time in PBS at 37 °C

	N/%				C/%				H/%			
	0 d	1 d	3 d	7 d	0 d	1 d	3 d	7 d	0 d	1 d	3 d	7 d
PLLA	0	0	0	0	51.54	49.39	50.76	49.66	6.12	5.79	5.99	5.92
PLLA–collagen	0.68	0.29	0.13	0.14	55.46	49.14	54.60	55.77	7.12	6.25	7.03	7.26
PLLA–chitosan	1.43	0.19	0.27	0.16	55.30	48.23	48.31	48.10	6.14	5.63	5.77	5.66

better mimics the parallel-aligned fibrils in the ECM of bones.[66] The alteration of PLLA fiber properties such as wettability, surface charge, and composition is expected to elicit the change in cellular behaviors such as cell adhesion and migration,[67] which shall be inspected in the next sessions.

3.4 Cell length, directional growth angle and viability

We found that in this study the cell length on the PLLA, PLLA–collagen and PLLA–chitosan scaffolds showed an obvious difference ($p < 0.01$) (Fig. 6a and b). The collagen or chitosan coated-scaffolds had larger cell length than the untreated PLLA scaffold, and the PLLA–collagen scaffold had the largest cell length. The collagen has a stronger ability to promote cell adhesion and growth,[68] facilitating cell penetration into the internal pores as well.[69]

The cell directional growth angles on the PLLA, PLLA–collagen and PLLA–chitosan scaffolds showed no obvious difference (Fig. 6c and d). All the aligned scaffolds could effectively guide cell growth along the parallel fiber arrangement direction. This is consistent with the previous observation that cells are directionally oriented along the dominant direction of parallel fibers,[4] mainly due to the contact guidance effect.[70]

The viability of osteoblasts on the PLLA melt spun fiber aligned scaffolds is shown in Fig. 6e. At 1 d, and the cell viability was the highest on the PLLA–chitosan scaffolds ($p < 0.01$ over PLLA fiber scaffolds, and $p < 0.05$ over PLLA–collagen scaffolds). The viability was enhanced on all the scaffolds on day 7, which was more significant on the PLLA–collagen and PLLA–chitosan scaffolds ($p < 0.01$ and $p < 0.05$ over PLLA fiber scaffolds, respectively). These results show that the collagen and chitosan coating is conductive to osteoblast proliferation,[60,71,72] and is effective in obtaining cytocompatible aligned scaffolds for mediating other cellular behaviors.

3.5 Cell morphology

Fig. 7 shows that macroscopically the cells were basically adhered onto the fibers and proliferated, and some others could proliferate between the fibers of the collagen or chitosan coated scaffolds. The actin fibers in the cells on the PLLA aligned scaffold showed a random and irregular distribution, conveying a weaker interaction between the cells and the fibers (Fig. 7a). By contrast, highly polarized and stressed actin fibers were formed in the cells on the collagen or chitosan coated fibers (Fig. 7b and c), especially on the PLLA–collagen scaffold (Fig. 7b), suggesting the stronger cell-substrate interaction. This is consistent with the functions of collagen and chitosan, which enhance the interaction between cells and substrates.[73] It is known that the actin fiber is a key factor in regulating the cell movement,[74] and plays an important role in cell adhesion.[75]

3.6 Cell directional migration

The cells migrated along the fiber axis of the aligned scaffolds with a bias direction along the fiber axis (Fig. 8a–c), and the migration distance on the position of the axis of PLLA–collagen and PLLA–chitosan aligned scaffolds was larger than on the untreated PLLA aligned scaffold. The migration rates of cells on the PLLA–collagen and PLLA–chitosan scaffolds were faster than that on the PLLA aligned scaffold ($p < 0.01$) (Fig. 8d). This is consistent with the cell morphology shown in Fig. 7 where the aligned cytoskeleton could enhance cell migration toward the parallel direction with a faster rate.[76] A previous study shows that on the aligned scaffolds the filopodia may extend out from the cells and penetrate into the surface layer of scaffolds.[4] This behavior would also benefit the cell migration from the scaffold surface into the internal pores of the scaffolds.

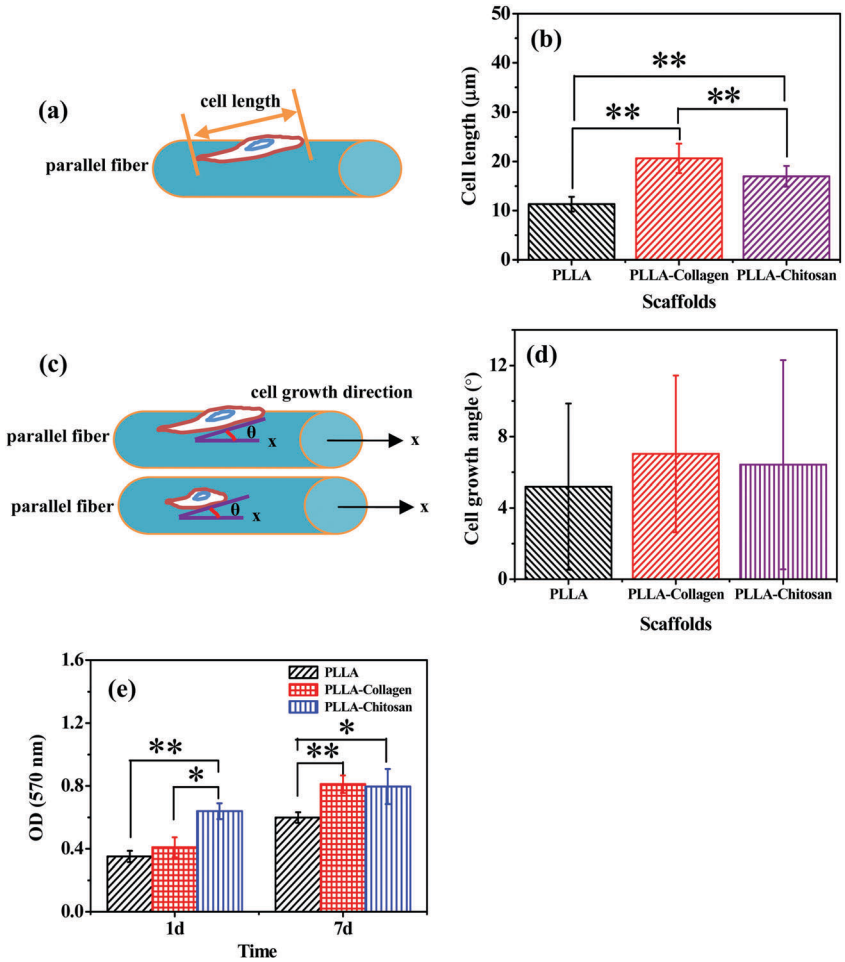

Fig. 6 (a) Schematic illustration of the measurement of cell length, (b) cell length on different types of scaffolds (N = 10), (c) schematic explanation showing the cell growth angle between cell growth direction and fiber parallel direction (fiber parallel direction was recorded as x axis), and (d) cell growth angle on different types of scaffolds (N = 10). (e) Cell viability (N = 3). * and ** indicate significant difference at $p < 0.05$ and $p < 0.01$, respectively.

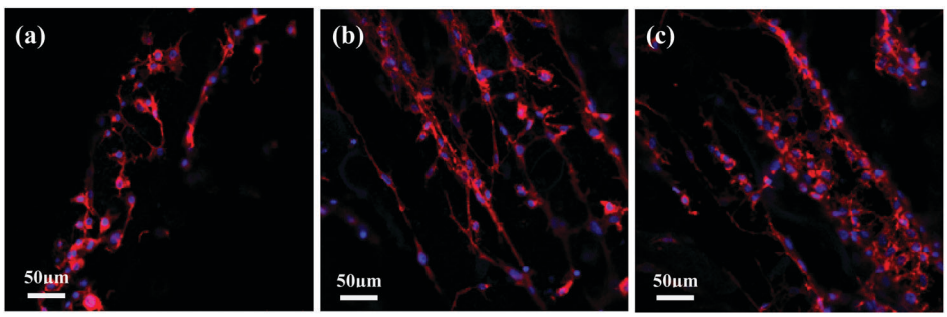

Fig. 7 CLSM images of osteoblasts on (a) PLLA, (b) PLLA–collagen and (c) PLLA–chitosan aligned scaffolds, respectively. Cell nuclei (blue) and actin fibers (red) were stained with blue and red color, respectively.

4. Discussion

Tissue engineering is involved in the implantation of a highly porous biomaterial scaffold populated with appropriate cells, providing a 3D environment in which new tissues can grow.[27] The aligned scaffolds simulate the aligned structure of ECM and play a pivotal role in controlling cell behaviors.[77] Bone is a natural organic–inorganic composite consisting of collagen fibrils and embedded, well-arrayed rod-like inorganic materials.[2,3] To more closely mimic ECM for bone tissue engineering, in this paper, PLLA melt spun fiber-aligned scaffolds were fabricated to modulate the behavior of osteoblasts.

PLLA fibers have been prepared by melt spinning,[78–80] wet spinning,[18] and electrospinning.[81] Persson *et al.*[78] prepared PLLA melt spun fibers and studied their thermal degradation,

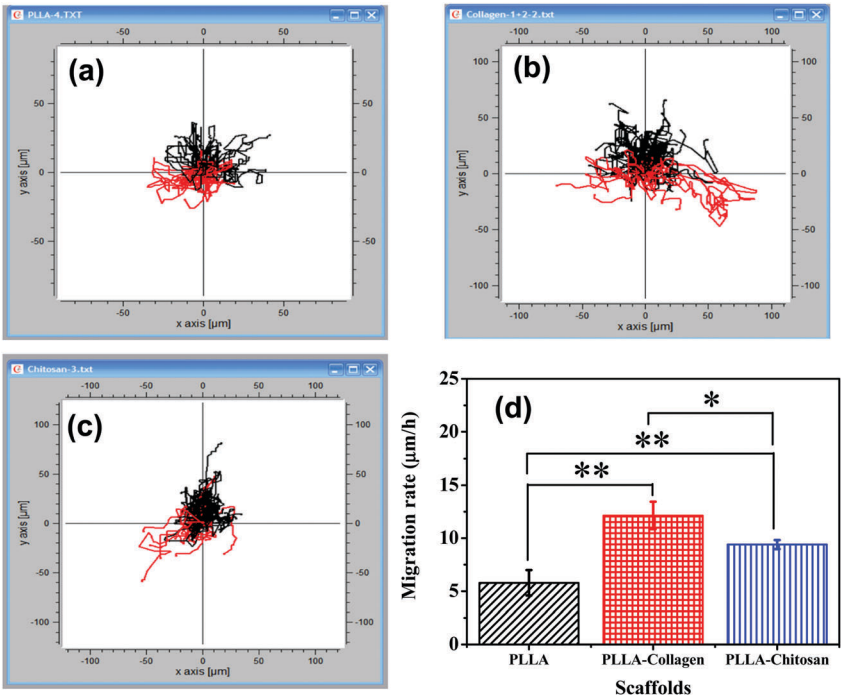

Fig. 8 Typical cell migration traces for 12 h on (a) PLLA, (b) PLLA–collagen, and (c) PLLA–chitosan aligned scaffolds. (d) Cell migration rate on three different scaffolds. At least 50 cells were tracked for each sample. The mobility of osteoblasts was continuously tracked every 15 min for 12 h after being cultured for 12 h. * and ** indicate significant difference at $p < 0.05$ and $p < 0.01$, respectively.

stability, thermal properties, crystallinity, mechanical properties, morphology and diameter. Zhang *et al.*[79] produced PLLA melt spun fibers by two-stage melt spinning processes and evaluated their surface morphology, melting curves, crystallinity, mechanical properties and heat resistance. Huang *et al.*[80] manufactured PLLA melt spun fibers by a melt-extruded method and analyzed the fiber morphology, melting peaks and glass transition temperature. Nelson *et al.*[18] manufactured PLLA wet spun fibers and studied their physical and mechanical properties, and molecular weight and crystallinity. In comparison with wet spinning and electrospinning, the melt spinning technology has the advantages of higher spinning speed, solvent-free processing and readily scalable production.[16]

PLLA fiber-aligned scaffolds have been mainly produced by the electrospinning method. For example, Zuidema *et al.*[82] produced PLLA nanofiber-aligned scaffolds for the repair of spinal cord injuries. Deepthi *et al.*[24] prepared PLLA nanofiber-aligned scaffolds for flexor tendon regeneration. Zhang *et al.*[54] used PLLA nanofiber-aligned scaffolds to promote neural cell growth, showing their potential applications in nerve tissue engineering. Andalib *et al.*[81] manufactured PLLA nanofiber-aligned scaffolds to regulate mesenchymal stem cell shape and other behaviors. Shalumon *et al.*[83] fabricated PLLA nanofiber-aligned scaffolds to control cellular organization in vascular tissue engineering. However, the aligned scaffolds prepared by the electrospinning technique have some obvious drawbacks, *i.e.*, a poorer bonding effect among fibers and limited production to meet the practical demands of tissue engineering.

The aligned scaffolds can be prepared by other methods such as freeze casting,[10] evaporation,[11] slip casting,[12] ice-templating,[13] centrifugal spinning,[25] melt-drawing,[26] unidirectional freeze-drying,[27] catalyst-free chemical vapor deposition,[28] 3D extrusion,[29] and bidirectional freezing.[30] Different from these literature studies, in this paper we produced PLLA melt spun fiber-aligned scaffolds by combination with a solvent bonding method. Through solvent bonding, the fiber parallel arrangement, pore structure and physical properties in the aligned scaffolds could be modulated by fiber parameters (diameter, number and direction), solvent parameters (solvent type and concentration) and drying process (temperature, time and pressure). To obtain the aligned scaffolds with better properties, a smaller number of PLLA melt spun fibers, a lower concentration of solvent and longer drying time should be used. After optimizing the experimental conditions, we used 70.3 ± 11.4 μm PLLA melt spun fibers and 5% PLLA tetrahydrofuran solution to prepare the porous and aligned fiber scaffolds.

To functionalize the PLLA fiber-aligned scaffolds, collagen and chitosan were coated onto the fibers/into the scaffolds, respectively. The PLLA–collagen and PLLA–chitosan aligned scaffolds had different alignment degrees, pore diameters and thicknesses in comparison with the uncoated PLLA aligned scaffold. The collagen and chitosan coating could improve cell growth significantly, which is well recognized since they both show better cytocompatibility than the PLLA substrate.[68] Due to different surface chemical properties, collagen- and chitosan-coated aligned scaffolds had larger cell length and migration rate than the untreated PLLA-aligned scaffold, and PLLA–collagen

aligned scaffold had the largest cell length and fastest migration rate. The collagen- and chitosan-coated PLLA-aligned scaffolds had multiple biochemical and surface-aligned topography cues, providing a versatile cell culture substrate to control cell behaviors so that the bone repair effect may be tailored *in vivo*. The improved osteoblast growth length is attributed to collagen molecules and collagen fibers that form the natural bone[84] with the target site of osteogenic cells.[85] The bionic surface of collagen-coated PLLA aligned scaffolds could also provide a suitable biomimetic microenvironment for osteoblast directional growth with larger viability. The structure of the aligned scaffolds is appropriate since usually a pore size of 20–1500 μm is beneficial for bone regeneration.[86]

Cell migration is a complicated process that is largely determined by the substrate, and is largely affected by various stimuli including biochemical and biophysical signals.[87] Cell migration is generally involves six sequential events: (1) sensing external motile stimuli by cell filopodia; (2) protrusion of lamellipodia and pseudopodia; (3) attachment of the protrusion to the extracellular matrix (ECM) *via* focal adhesion; (4) stress fiber-mediated contraction of the cell body to allow forward movement; (5) rear release by stress fiber-mediated traction forces; and (6) repeating the adhesion and signaling materials.[88] The collagen or chitosan-coated PLLA aligned scaffolds had multiple biochemical and surface aligned topography cues, providing a versatile cell culture substrate to control cell behaviors. The composite artificial ECM consisted of different surface topographies of aligned PLLA melt spun fibers and the chemical characteristics of collagen could regulate cell migration and guide cell growth along the fiber parallel direction. The larger osteoblast migration rate in the PLLA–collagen scaffold suggests that it would be a better substrate for bone regeneration.[89]

5. Conclusions

Solvent-bonded PLLA melt spun fiber-aligned scaffolds were prepared, and were further coated with collagen or chitosan to obtain the cytocompatible aligned scaffolds. Compared with the uncoated aligned scaffolds, the collagen- or chitosan-coated aligned scaffolds had better cell response in terms of adhesion, viability, length and migration. The collagen-coated aligned scaffold had larger cell length and migration rate, and the osteoblasts preferentially migrated and grew along the parallel fiber direction. The bionic surface of collagen-coated PLLA aligned scaffolds could provide a suitable biomimetic microenvironment for osteoblast directional growth and migration, showing great potential for bone regeneration.

Acknowledgements

This study is financially supported by the Natural Science Foundation of China (21434006, 21374097), Zhejiang Sci-Tech University Scientific Research Project (16012055-Y), and Key Laboratory of Advanced Textile Materials and Manufacturing Technology (Zhejiang Sci-Tech University), Ministry of Education (2016QN06).

References

1 S. Patel, K. Kurpinski, R. Quigley, H. F. Gao, B. S. Hsiao and M. M. Poo, *et al.*, Bioactive nanofibers: Synergistic effects of nanotopography and chemical signaling on cell guidance, *Nano Lett.*, 2007, **7**, 2122–2128.
2 G. E. Poinern, R. K. Brundavanam, N. Mondinos and Z. T. Jiang, Synthesis and characterisation of nanohydroxyapatite using an ultrasound assisted method, *Ultrason. Sonochem.*, 2009, **16**, 469–474.
3 H. Zhou and J. Lee, Nanoscale hydroxyapatite particles for bone tissue engineering, *Acta Biomater.*, 2011, **7**, 2769–2781.
4 H. B. Chen, Y. Z. Qian, Y. Xia, G. Chen, Y. Dai and N. Li, *et al.*, Enhanced Osteogenesis of ADSCs by the Synergistic Effect of Aligned Fibers Containing Collagen I, *ACS Appl. Mater. Interfaces*, 2016, **8**, 29289–29297.
5 M. Kharaziha, M. H. Fathi and H. Edris, Development of novel aligned nanofibrous composite membranes for guided bone regeneration, *J. Mech. Behav. Biomed. Mater.*, 2013, **24**, 9–20.
6 S. K. M. Perikamana, J. Lee, T. Ahmad, Y. Jeong, D. G. Kim and K. Kim, *et al.*, Effects of Immobilized BMP-2 and Nanofiber Morphology on In Vitro Osteogenic Differentiation of hMSCs and In Vivo Collagen Assembly of Regenerated Bone, *ACS Appl. Mater. Interfaces*, 2015, **7**, 8798–8808.
7 W. L. Shao, J. X. He, F. Sang, B. Ding, L. Chen and S. Z. Cui, *et al.*, Coaxial electrospun aligned tussah silk fibroin nanostructured fiber scaffolds embedded with hydroxyapatite-tussah silk fibroin nanoparticles for bone tissue engineering, *Mater. Sci. Eng., C*, 2016, **58**, 342–351.
8 B. Lanfer, F. P. Seib, U. Freudenberg, D. Stamov, T. Bley and M. Bornhäuser, *et al.*, The growth and differentiation of mesenchymal stem and progenitor cells cultured on aligned collagen matrices, *Biomaterials*, 2009, **30**, 5950–5958.
9 Y. H. Hu, J. O. You and J. Aizenberg, Micropatterned Hydrogel Surface with High-Aspect-Ratio Features for Cell Guidance and Tissue Growth, *ACS Appl. Mater. Interfaces*, 2016, **8**, 21939–21945.
10 Z. Wang, P. Z. Feng, X. H. Wang, P. Geng, F. Akhtar and H. F. Zhang, Fabrication and properties of freeze-cast mullite foams derived from coal-series kaolin, *Ceram. Interfaces*, 2016, **42**, 12414–12421.
11 S. D. Frazier and W. V. Srubar, Evaporation-based method for preparing gelatin foams with aligned tubular pore structures, *Mater. Sci. Eng., C*, 2016, **62**, 467–473.
12 F. Sarhadi, M. S. Afarani, D. Mohebbi-Kalhori and M. Shayesteh, Fabrication of alumina porous scaffolds with aligned oriented pores for bone tissue engineering applications, *Appl. Phys. A: Mater. Sci. Process.*, 2016, **122**, 1–8.
13 B. L. Liu, L. J. Chen, C. S. Shao, F. Q. Zhang, K. C. Zhou and J. Cao, *et al.*, Improved osteoblasts growth on osteomimetic hydroxyapatite/$BaTiO_3$ composites with aligned lamellar porous structure, *Mater. Sci. Eng., C*, 2016, **61**, 8–14.
14 A. Patel, S. Mukundan, W. H. Wang, A. Karumuri, V. Sant and S. M. Mukhopadhyay, *et al.*, Carbon-based hierarchical scaffolds for myoblast differentiation: Synergy between

nano-functionalization and alignment, *Acta Biomater.*, 2016, **32**, 77–88.

15 S. H. Park, M. S. Kim, B. Lee, J. H. Park, H. J. Lee and N. K. Lee, *et al.*, Creation of a Hybrid Scaffold with Dual Configuration of Aligned and Random Electrospun Fibers, *ACS Appl. Mater. Interfaces*, 2016, **8**, 2826–2832.

16 M. Persson, S. W. Cho and M. Skrifvars, The effect of process variables on the properties of melt-spun poly-(lactic acid) fibres for potential use as scaffold matrix materials, *J. Mater. Sci.*, 2013, **48**, 3055–3066.

17 L. Fambri, A. Pegoretti, M. Mazzurana and C. Migliaresi, Biodegradable Fibers. 1. Poly-L-Lactic Acid Fibers Produced by Solution Spinning, *J. Mater. Sci.: Mater. Med.*, 1994, **5**, 679–683.

18 K. D. Nelson, A. Romero, P. Waggoner, B. Crow, A. Borneman and G. M. Smith, Technique paper for wet-spinning Poly(L-lactic acid) and poly(DL-lactide-*co*-glycolide) monofilament fibers, *Tissue Eng.*, 2003, **9**, 1323–1330.

19 B. Gupta, N. Revagade, N. Anjum, B. Atthoff and J. Hilborn, Preparation of poly(lactic acid) fiber by dry-jet-wet-spinning. I. Influence of draw ratio on fiber properties, *J. Appl. Polym. Sci.*, 2006, **100**, 1239–1246.

20 B. Gupta, N. Revagade, N. Anjum, B. Atthoff and J. Hilborn, Preparation of poly(lactic acid) fiber by dry-jet-wet spinning. II. Effect of process parameters on fiber properties, *J. Appl. Polym. Sci.*, 2006, **101**, 3774–3780.

21 H. C. Chen, C. H. Tsai and M. C. Yang, Mechanical properties and biocompatibility of electrospun polylactide/poly(vinylidene fluoride) mats, *J. Polym. Res.*, 2011, **18**, 319–327.

22 L. M. He, S. S. Liao, D. P. Quan, K. Ma, C. Chan and S. Ramakrishna, *et al.*, Synergistic effects of electrospun PLLA fiber dimension and pattern on neonatal mouse cerebellum C17.2 stem cells, *Acta Biomater.*, 2010, **6**, 2960–2969.

23 C. Xu, R. Inai, M. Kotaki and S. Ramakrishna, Aligned biodegradable nanofibrous structure: a potential scaffold for blood vessel engineering, *Biomaterials*, 2004, **25**, 877–886.

24 S. Deepthi, M. N. Sundaram, J. D. Kadavan and R. Jayakumar, Layered chitosan–collagen hydrogel/aligned PLLA nanofiber construct for flexor tendon regeneration, *Carbohydr. Polym.*, 2016, **153**, 492–500.

25 L. Wang, M. W. Chang, Z. Ahmad, H. X. Zheng and J. S. Li, Mass and controlled fabrication of aligned PVP fibers for matrix type antibiotic drug delivery systems, *Chem. Eng. J.*, 2017, **307**, 661–669.

26 Y. J. Tan, X. Tan, W. Y. Yeong and S. B. Tor, Additive Manufacturing of Patient-Customizable Scaffolds for Tubular Tissues Using the Melt-Drawing Method, *Materials*, 2016, **9**, 1–13.

27 Z. Fereshteh, M. Fathi, A. Bagri and A. R. Boccaccini, Preparation and characterization of aligned porous PCL/zein scaffolds as drug delivery systems *via* improved unidirectional freeze-drying method, *Mater. Sci. Eng., C*, 2016, **68**, 613–622.

28 J. Kazantseva, R. Ivanov, M. Gasik, T. Neuman and I. Hussainova, Graphene-augmented nanofiber scaffolds demonstrate new features in cells behaviour, *Sci. Rep.*, 2016, **6**, 1–8.

29 Y. W. Moon, I. J. Choi, Y. H. Koh and H. E. Kim, Porous alumina ceramic scaffolds with biomimetic macro/micro-porous structure using three-dimensional (3-D) ceramic/camphene-based extrusion, *Ceram. Interfaces*, 2015, **41**, 12371–12377.

30 H. Bai, F. Walsh, B. Gludovatz, B. Delattre, C. L. Huang and Y. Chen, *et al.*, Bioinspired Hydroxyapatite/Poly(methyl methacrylate) Composite with a Nacre-Mimetic Architecture by a Bidirectional Freezing Method, *Adv. Mater.*, 2016, **28**, 50–56.

31 U. Stachewicz, T. Qiao, S. C. Rawlinson, F. V. Almeida, W.-Q. Li and M. Cattell, *et al.*, 3D imaging of cell interactions with electrospun PLGA nanofiber membranes for bone regeneration, *Acta Biomater.*, 2015, **27**, 88–100.

32 S. Samavedi, P. Vaidya, P. Gaddam, A. R. Whittington and A. S. Goldstein, Electrospun Meshes Possessing Region-Wise Differences in Fiber Orientation, Diameter, Chemistry and Mechanical Properties for Engineering Bone–Ligament–Bone Tissues, *Biotechnol. Bioeng.*, 2014, **111**, 2549–2559.

33 E. Antonioli, A. O. Lobo, M. Ferretti, M. Cohen, F. R. Marciano and E. J. Corat, *et al.*, An evaluation of chondrocyte morphology and gene expression on superhydrophilic vertically-aligned multi-walled carbon nanotube films, *Mater. Sci. Eng., C*, 2013, **33**, 641–647.

34 Z. W. Ma, Z. W. Mao and C. Y. Gao, Surface modification and property analysis of biomedical polymers used for tissue engineering, *Colloids Surf., B*, 2007, **60**, 137–157.

35 L. Sun, C. C. Berndt, K. A. Gross and A. Kucuk, Material fundamentals and clinical performance of plasma-sprayed hydroxyapatite coatings: a review, *J. Biomed. Mater. Res.*, 2001, **58**, 570–592.

36 Y. Yang, K.-H. Kim and J. L. Ong, A review on calcium phosphate coatings produced using a sputtering process—an alternative to plasma spraying, *Biomaterials*, 2005, **26**, 327–337.

37 A. Motealleh, S. Eqtesadi, F. H. Perera, A. Pajares, F. Guiberteau and P. Miranda, Understanding the role of dip-coating process parameters in the mechanical performance of polymer-coated bioglass robocast scaffolds, *J. Mech. Behav. Biomed. Mater.*, 2016, **64**, 253–261.

38 B. Holmes, X. Q. Fang, A. Zarate, M. Keidar and L. G. Zhang, Enhanced human bone marrow mesenchymal stem cell chondrogenic differentiation in electrospun constructs with carbon nanomaterials, *Carbon*, 2016, **97**, 1–13.

39 W. A. R. Neto, A. C. C. de Paula, T. M. M. Martins, A. M. Goes, L. Averous and G. Schlatter, *et al.*, Poly(butylene adipate-*co*-terephthalate)/hydroxyapatite composite structures for bone tissue recovery, *Polym. Degrad. Stab.*, 2015, **120**, 61–69.

40 A. E. Sorkio, E. P. Vuorimaa-Laukkanen, H. M. Hakola, H. Liang, T. A. Ujula and J. J. Valle-Delgado, *et al.*, Biomimetic collagen I and IV double layer Langmuir–Schaefer films as microenvironment for human pluripotent stem cell derived retinal pigment epithelial cells, *Biomaterials*, 2015, **51**, 257–269.

41 X.-Y. Ma, Y.-F. Feng, Z.-S. Ma, X. Li, J. Wang and L. Wang, *et al.*, The promotion of osteointegration under diabetic

conditions using chitosan/hydroxyapatite composite coating on porous titanium surfaces, *Biomaterials*, 2014, **35**, 7259–7270.

42 W. Hu, Z. M. Huang and X. Y. Liu, Development of braided drug-loaded nanofiber sutures, *Nanotechnology*, 2010, **21**, 1–11.

43 D. R. Nisbet, A. E. Rodda, M. K. Horne, J. S. Forsythe and D. I. Finkelstein, Neurite infiltration and cellular response to electrospun polycaprolactone scaffolds implanted into the brain, *Biomaterials*, 2009, **30**, 4573–4580.

44 C. Guo and L. J. Kaufman, Flow and magnetic field induced collagen alignment, *Biomaterials*, 2007, **28**, 1105–1114.

45 C. Ayres, G. L. Bowlin, S. C. Henderson, L. Taylor, J. Shultz and J. Alexander, *et al.*, Modulation of anisotropy in electrospun tissue-engineering scaffolds: analysis of fiber alignment by the fast Fourier transform, *Biomaterials*, 2006, **27**, 5524–5534.

46 C. H. Lee, H. J. Shin, I. H. Cho, Y.-M. Kang, I. A. Kim and K.-D. Park, *et al.*, Nanofiber alignment and direction of mechanical strain affect the ECM production of human ACL fibroblast, *Biomaterials*, 2005, **26**, 1261–1270.

47 R. Nazarov, H. J. Jin and D. L. Kaplan, Porous 3-D scaffolds from regenerated silk fibroin, *Biomacromolecules*, 2004, **5**, 718–726.

48 Y. Zhu, Z. Mao and C. Gao, Control over the gradient differentiation of rat BMSCs on a PCL membrane with surface-immobilized alendronate gradient, *Biomacromolecules*, 2013, **14**, 342–349.

49 P. Jiang, Z. Mao and C. Gao, Combinational effect of matrix elasticity and alendronate density on differentiation of rat mesenchymal stem cells, *Acta Biomater.*, 2015, **19**, 76–84.

50 T. Ren, S. Yu, Z. Mao, S. E. Moya, L. Han and C. Gao, Complementary density gradient of poly(hydroxyethyl methacrylate) and YIGSR selectively guides migration of endotheliocytes, *Biomacromolecules*, 2014, **15**, 2256–2264.

51 F. Yang, R. Murugan, S. Wang and S. Ramakrishna, Electrospinning of nano/micro scale poly(L-lactic acid) aligned fibers and their potential in neural tissue engineering, *Biomaterials*, 2005, **26**, 2603–2610.

52 S. Yu, Z. W. Mao and C. Y. Gao, Preparation of gelatin density gradient on poly(epsilon-caprolactone) membrane and its influence on adhesion and migration of endothelial cells, *J. Colloid Interface Sci.*, 2015, **451**, 177–183.

53 P. Jiang, D. Yu, W. Zhang, Z. Mao and C. Gao, Influence of bovine serum albumin coated poly(lactic-*co*-glycolic acid) particles on differentiation of mesenchymal stem cells, *RSC Adv.*, 2015, **5**, 40924–40931.

54 K. H. Zhang, H. H. Zheng, S. Liang and C. Y. Gao, Aligned PLLA nanofibrous scaffolds coated with graphene oxide for promoting neural cell growth, *Acta Biomater.*, 2016, **37**, 131–142.

55 T. C. Ren, S. Yu, Z. W. Mao and C. Y. Gao, A complementary density gradient of zwitterionic polymer brushes and NCAM peptides for selectively controlling directional migration of Schwann cells, *Biomaterials*, 2015, **56**, 58–67.

56 J. Deng, S. Wu, M. Y. Yao and C. Y. Gao, Surface-anchored poly(acryloyl-L(D)-valine) with enhanced chirality-selective effect on cellular uptake of gold nanoparticles, *Sci. Rep.*, 2016, **6**, 31595.

57 Y. Nishimura, A. Takasu, Y. Inai and T. Hirabayashi, Melt spinning of poly(L-lactic acid) and its biodegradability, *J. Appl. Polym. Sci.*, 2005, **97**, 2118–2124.

58 X. Yuan, A. F. Mak, K. Kwok, B. K. Yung and K. Yao, Characterization of poly(L-lactic acid) fibers produced by melt spinning, *J. Appl. Polym. Sci.*, 2001, **81**, 251–260.

59 A. J. Salgado, O. P. Coutinho and R. L. Reis, Bone tissue engineering: state of the art and future trends, *Macromol. Biosci.*, 2004, **4**, 743–765.

60 X. Fu, M. Xu, J. Liu, Y. Qi, S. Li and H. Wang, Regulation of migratory activity of human keratinocytes by topography of multiscale collagen-containing nanofibrous matrices, *Biomaterials*, 2014, **35**, 1496–1506.

61 C.-C. Lin, S.-J. Fu, Y.-C. Lin, I.-K. Yang and Y. Gu, Chitosan-coated electrospun PLA fibers for rapid mineralization of calcium phosphate, *Int. J. Biol. Macromol.*, 2014, **68**, 39–47.

62 T. Douglas and H. J. Haugen, Coating of polyurethane scaffolds with collagen: comparison of coating and cross-linking techniques, *J. Mater. Sci.: Mater. Med.*, 2008, **19**, 2713–2719.

63 H. Bocherens, D. G. Drucker and H. Taubald, Preservation of bone collagen sulphur isotopic compositions in an early Holocene river-bank archaeological site, *Palaeogeogr., Palaeoclimatol., Palaeoecol.*, 2011, **310**, 32–38.

64 A. Sliwak, N. Diez, E. Miniach and G. Gryglewicz, Nitrogen-containing chitosan-based carbon as an electrode material for high-performance supercapacitors, *J. Appl. Electrochem.*, 2016, **46**, 667–677.

65 J. N. Harvestine, N. L. Vollmer, S. S. Ho, C. A. Zikry, M. A. Lee and J. K. Leach, Extracellular Matrix-Coated Composite Scaffolds Promote Mesenchymal Stem Cell Persistence and Osteogenesis, *Biomacromolecules*, 2016, **17**, 3524–3531.

66 G. Chen, J. L. Chen, B. Yang, L. Li, X. Y. Luo and X. X. Zhang, *et al.*, Combination of aligned PLGA/Gelatin electrospun sheets, native dental pulp extracellular matrix and treated dentin matrix as substrates for tooth root regeneration, *Biomaterials*, 2015, **52**, 56–70.

67 M. Padial-Molina, P. Galindo-Moreno, J. E. Fernandez-Barbero, F. O'Valle, A. B. Jodar-Reyes and J. L. Ortega-Vinuesa, *et al.*, Role of wettability and nanoroughness on interactions between osteoblast and modified silicon surfaces, *Acta Biomater.*, 2011, **7**, 771–778.

68 F. J. O'Brien, B. Harley, I. V. Yannas and L. J. Gibson, The effect of pore size on cell adhesion in collagen-GAG scaffolds, *Biomaterials*, 2005, **26**, 433–441.

69 A. S. Badami, M. R. Kreke, M. S. Thompson, J. S. Riffle and A. S. Goldstein, Effect of fiber diameter on spreading, proliferation, and differentiation of osteoblastic cells on electrospun poly(lactic acid) substrates, *Biomaterials*, 2006, **27**, 596–606.

70 F. Laco, M. H. Grant and R. A. Black, Collagen–nanofiber hydrogel composites promote contact guidance of human lymphatic microvascular endothelial cells and directed

capillary tube formation, *J. Biomed. Mater. Res., Part A*, 2013, **101**, 1787–1799.

71 M. Maldonado, L. Y. Wong, C. Echeverria, G. Ico, K. Low and T. Fujimoto, *et al.*, The effects of electrospun substrate-mediated cell colony morphology on the self-renewal of human induced pluripotent stem cells, *Biomaterials*, 2015, **50**, 10–19.

72 C. S. Wong, X. Liu, Z. Xu, T. Lin and X. Wang, Elastin and collagen enhances electrospun aligned polyurethane as scaffolds for vascular graft, *J. Mater. Sci.: Mater. Med.*, 2013, **24**, 1865–1874.

73 C. P. Pennisi, A. Dolatshahi-Pirouz, M. Foss, J. Chevallier, T. Fink and V. Zachar, *et al.*, Nanoscale topography reduces fibroblast growth, focal adhesion size and migration-related gene expression on platinum surfaces, *Colloids Surf., B*, 2011, **85**, 189–197.

74 R. Dominguez and K. C. Holmes, Actin structure and function, *Annu. Rev. Biophys.*, 2011, **40**, 169.

75 S. Kim, K. Shilagardi, S. Zhang, S. N. Hong, K. L. Sens and J. Bo, *et al.*, A critical function for the actin cytoskeleton in targeted exocytosis of prefusion vesicles during myoblast fusion, *Dev. Cell*, 2007, **12**, 571–586.

76 J. M. Zuidema, M. C. Hyzinski-García, K. Van Vlasselaer, N. W. Zaccor, G. E. Plopper and A. A. Mongin, *et al.*, Enhanced GLT-1 mediated glutamate uptake and migration of primary astrocytes directed by fibronectin-coated electrospun poly-L-lactic acid fibers, *Biomaterials*, 2014, **35**, 1439–1449.

77 L. Ghasemi-Mobarakeh, M. P. Prabhakaran, M. Morshed, M. H. Nasr-Esfahani and S. Ramakrishna, Electrospun poly(epsilon-caprolactone)/gelatin nanofibrous scaffolds for nerve tissue engineering, *Biomaterials*, 2008, **29**, 4532–4539.

78 M. Persson, S.-W. Cho and M. Skrifvars, The effect of process variables on the properties of melt-spun poly(lactic acid) fibres for potential use as scaffold matrix materials, *J. Mater. Sci.*, 2013, **48**, 3055–3066.

79 H. X. Zhang, H. W. Bai, Z. W. Liu, Q. Zhang and Q. Fu, Toward High-Performance Poly(L-lactide) Fibers *via* Tailoring Crystallization with the Aid of Fibrillar Nucleating Agent, *ACS Sustainable Chem. Eng.*, 2016, **4**, 3939–3947.

80 W. Huang, X. Z. Luo, B. J. Wang, W. F. Wei, P. Chen and Q. Gu, *et al.*, Nanostructures of Stereocomplex Polylactide in Poly(L-lactide) Doped with Poly(D-lactide), *Macromol. Chem. Phys.*, 2015, **216**, 1120–1124.

81 M. N. Andalib, J. S. Lee, L. Ha, Y. Dzenis and J. Y. Lim, Focal adhesion kinase regulation in stem cell alignment and spreading on nanofibers, *Biochem. Biophys. Res. Commun.*, 2016, **473**, 920–925.

82 J. M. Zuidema, G. P. Desmond, C. J. Rivet, K. R. Kearns, D. M. Thompson and R. J. Gilbert, Nebulized solvent ablation of aligned PLLA fibers for the study of neurite response to anisotropic-to-isotropic fiber/film transition (AFFT) boundaries in astrocyte-neuron co-cultures, *Biomaterials*, 2015, **46**, 82–94.

83 K. T. Shalumon, S. Deepthi, M. S. Anupama, S. V. Nair, R. Jayakumar and K. P. Chennazhi, Fabrication of poly(L-lactic acid)/gelatin composite tubular scaffolds for vascular tissue engineering, *Int. J. Biol. Macromol.*, 2015, **72**, 1048–1055.

84 Y. Chen, A. F. Mak, M. Wang, J. Li and M. Wong, PLLA scaffolds with biomimetic apatite coating and biomimetic apatite/collagen composite coating to enhance osteoblast-like cells attachment and activity, *Surf. Coat. Technol.*, 2006, **201**, 575–580.

85 T. Douglas, S. Heinemann, U. Hempel, C. Mietrach, C. Knieb and S. Bierbaum, *et al.*, Characterization of collagen II fibrils containing biglycan and their effect as a coating on osteoblast adhesion and proliferation, *J. Mater. Sci.: Mater. Med.*, 2008, **19**, 1653–1660.

86 C. M. Murphy, M. G. Haugh and F. J. O'Brien, The effect of mean pore size on cell attachment, proliferation and migration in collagen–glycosaminoglycan scaffolds for bone tissue engineering, *Biomaterials*, 2010, **31**, 461–466.

87 T. T. Li, K. Xu, Y. Fu and K. Y. Cai, Inducing the migration behavior of endothelial cells by tuning the ligand density on a density-gradient poly(ethylene glycol) surface, *Colloids Surf., B*, 2016, **143**, 557–564.

88 P. Wu, Y. Fu and K. Y. Cai, Regulation of the migration of endothelial cells by a gradient density of vascular endothelial growth factor, *Colloids Surf., B*, 2014, **123**, 181–190.

89 L. M. Yu, Q. S. Tu, Q. Q. Han, L. Zhang, L. Sui and L. L. Zheng, *et al.*, Adiponectin Regulates Bone Marrow Mesenchymal Stem Cell Niche Through a Unique Signal Transduction Pathway: An Approach for Treating Bone Disease in Diabetes, *Stem Cells*, 2015, **33**, 240–252.

